Surface pressure and elevation correction from observation and multiple reanalyses over the Tibetan Plateau

Qinglong You [1]*, Yuntao Bao[2], Zhihong Jiang[2], Nick Pepin[3], G.W.K. Moore[4]

1. Department of Atmospheric and Oceanic Sciences & Institute of Atmospheric Sciences, Fudan University, 200438, Shanghai, China;

2. Key Laboratory of Meteorological Disaster, Ministry of Education (KLME), Nanjing University of Information Science and Technology (NUIST), Nanjing, 210044, China;

3. Department of Geography, University of Portsmouth, PO1 3HE, U.K.

4. Department of Physics, University of Toronto, Toronto, Ontario, Canada;

* Corresponding author E-mail address: yqingl@126.com

Abstract: Surface pressure reflects the deep structure of the overlying atmosphere, and is recognized as an indicator of climate change. In this study, observed surface pressure at 71 stations over the Tibetan Plateau (TP) during 1979-2013 is analyzed and compared with monthly means from multiple reanalyses (NCEP1, NCEP2, ERA-Interim, MERRA and JRA55). During the studied period, surface pressure from both observations and the reanalyses increases slowly up until the mid-2000s but shows a decrease afterwards, leading to a recent fall in pressure. However, the surface pressure over the TP in spring has increased, probably explained by the thermal condition such as diabatic heating change. Observations and the multiple reanalyses are positively correlated at most locations indicating that reanalyses reproduce the interannual variation and long-term trend of observed surface pressure fairly well. Despite high inter-annual correlation, trend magnitudes over 1979-2013 are varied, with observations showing decreased pressure at most stations, but reanalyses showing increases in many cases. Compared with observations however, surface pressures from all reanalyses are underestimated usually by about 3-6%. There are significant positive correlations between surface pressure bias and elevation bias, suggesting that overestimation of elevation partially explains the surface pressure bias. A topographical correction method using the hydrostatic equation is therefore conducted and more than 90% of the biases of the reanalyses can be eliminated. Overall, this study points to the importance of better analyzing the importance of topography in the western TP to enhance understanding of reanalysis uncertainties in this region.

Key words: Tibetan Plateau; Surface pressure; Multiple reanalyses; Trend

1. Introduction

Due to the extensive area of high terrain, the Tibetan Plateau (TP) exerts a strong influence on regional and global atmospheric circulation and climate, particularly in central and eastern Asia through both mechanical and thermal forcing [*Duan et al.*, 2012; *Liu et al.*, 2009; *G X Wu et al.*, 2015; *Yang et al.*, 2014; *Yang et al.*, 2011; *You et al.*, 2017; *You et al.*, 2015a]. In summer, the TP serves as a significant heat source, and plays a unique role in controlling the development of the Asian summer monsoon and resultant weather systems over the whole of China. This has been examined through numerical simulations, numerous data analyses and theoretical studies [*Duan et al.*, 2012; *Duan and Wu*, 2005; *Rangwala et al.*, 2010; *G X Wu et al.*, 2015; *Yanai and Li*, 1994; *Yanai et al.*, 1992; *You et al.*, 2015a; *You et al.*, 2013c]. Surface heating can trigger deep convection above the TP which supports exchange of water vapor and air pollutants between the troposphere and stratosphere [*Fu et al.*, 2006]. In winter, the TP acts as an elevated cold land surface for snow/ice accumulation and glacier development, and provides a water source for the Asian population [*Barnett et al.*, 2005]. Previous studies have shown a close relationship between winter snow/glacier accumulation in the TP and the intensity of the following Indian/East Asian summer monsoon [*Hahn and Shukla*, 1976; *Moore*, 2012; *T W Wu and Qian*, 2003]. For example there are clear positive correlations between snow cover over the TP and subsequent summer rainfall over the middle and lower reaches of the Yangtze River valley (central China) [*T W Wu and Qian*, 2003]. However, long term climate and cryospheric changes over the TP have altered atmospheric and hydrological cycles and

61 reshaped the local environment [*Kang et al.*, 2010; *Yang et al.*, 2014; *Yang et al.*, 2011;
62 *You et al.*, 2013a; *You et al.*, 2013b]. Our understanding of climate change over the TP
63 has been significantly advanced in the recent decades due to improvements in both
64 observational data and numerical models [*Cai et al.*, 2017; *Cuo et al.*, 2013; *Kang et*
65 *al.*, 2010; *Liu et al.*, 2009; *G X Wu et al.*, 2015; *Yang et al.*, 2014]. In addition to models
66 and observations, reanalyses are also an important data source, and are used extensively
67 in the study of weather and climate, due to their consistent temporal and spatial
68 resolution [*Dee et al.*, 2011; *Kobayashi et al.*, 2015; *Rienecker et al.*, 2011]. However,
69 reanalyses require systematic evaluation of their quality before extending their
70 application [*Bao and Zhang*, 2013; *Ma et al.*, 2008; *You et al.*, 2013a].

71 Surface pressure is an easily measured field and relatively insensitive to local-scale
72 features, and can therefore be representative of large-scale atmospheric conditions.
73 Furthermore, the first source of variation in surface pressure comes from topography,
74 which is location-dependent [*Compo et al.*, 2006; *Hahn and Shukla*, 1976; *Moore*, 2012;
75 *You et al.*, 2017]. The annual mean cycle and inter-annual variability of surface pressure
76 can be analyzed to depict the state of the climate system [*Chen et al.*, 1997; *Cullather*
77 *and Lynch*, 2003; *Han et al.*, 2010; *Trenberth*, 1981; *van den Dool and Saha*, 1993;
78 *Zishka and Smith*, 1980]. Previous studies show that changes in surface pressure are
79 associated with a wide range of atmospheric phenomena, such as mesoscale gravity
80 waves, convective complexes, and synoptic disturbances [*Jacques et al.*, 2015; *Koppel*
81 *et al.*, 2000]. In addition, compared with temperature and wind measurements, surface
82 pressure observations have fewer siting and measurement issues [*Mass and Madaus*,

2014], which makes them readily assimilated into operational models [*Mass and Madaus*, 2014; *Wheatley and Stensrud*, 2010]. Assimilation of surface pressure observations is non-trivial in high-altitude terrain, and the adjustment to station altitude is of great importance when considering the pressure observations [*Ingleby*, 2015]. Therefore, numerous studies have relied on pressure observations to catalogue and examine climate change [*e.g., Toumi et al.*, 1999], changes in atmospheric or oceanic circulation [*e.g., Han et al.*, 2010], synoptic storm tracks [*e.g., Zishka and Smith*, 1980] and the total mass of the atmosphere [*e.g., Trenberth,* 1981]. Changes in surface pressure not only test the reliability of climate models but also facilitate understanding of the atmosphere as a whole [*Van Wijngaarden*, 2005] because surface pressure reflects the overlying structure of the whole atmospheric column [*Mass and Madaus*, 2014].

Considerable efforts to obtain more reliable estimates of surface pressure have been performed on global and regional scales [*Chen et al.*, 1997; *Moore*, 2012; *Toumi et al.*, 1999; *Trenberth et al.*, 1987; *Van Wijngaarden*, 2005], including studies of the Hadley Center historical gridded global monthly mean sea level pressure (HadSLP) [*Allan and Ansell*, 2006], the Arctic [*Gillett et al.*, 2003], the Canadian Arctic [*Gillett et al.*, 2003; *Van Wijngaarden*, 2005], the United States [*Jacques et al.*, 2015; *Koppel et al.*, 2000], the Southern Ocean and Antarctica [*Hines et al.*, 2000], the Tibetan Plateau [*Moore*, 2012; *You et al.*, 2017], and the Indian Ocean [*Gillett et al.*, 2003]. It has been shown that surface pressure in the Arctic region has decreased by 4 hPa during winter over the period 1968–1997 [*Gillett et al.*, 2003]. Over the Canadian Arctic in winter, the surface

pressure has decreased by 3-4 hPa during 1948–1998 [*Gillett et al.*, 2003], confirmed by the fact that surface pressure during 1953–2003 has shown a statistically significant decrease in the same region [*Van Wijngaarden*, 2005].

Over the TP, surface pressure is low/high when surface temperature is low/high, partly because of the high elevation. This is in contrast to many lowland areas, particularly on mid-latitude continents where the reverse can be the case because of the association of anticyclones with cold air in winter [*Saha et al.*, 1994; *van den Dool and Saha*, 1993]. Several studies have documented the variability of surface pressure over the TP, with particular interest in patterns during the south Asian monsoon [*G X Wu et al.*, 2015; *Yanai et al.*, 1992] and TP monsoon [*Kang et al.*, 2010]. These questions are crucial to understanding not only ground/surface climate change but also the structure of the upper-air over the TP. Surface pressure can be used to yield a reasonable approximation of circulation where flow is barotropic, in turn allowing development of indices representing amplitudes and phases of various atmospheric modes [*Compo et al.*, 2006; *Trenberth et al.*, 1987].

In this study, the variability of surface pressure across the TP is analyzed using monthly means from station observations and multiple reanalyses. The purpose of this study is to address the following questions:

(1) What is the variability of observed surface pressure over the TP?

(2) How well do the multiple reanalyses reproduce the observed pressure across the TP?

125 (3) What are the reasons for discrepancies between observations and reanalyses?

126 This study is organized as follows: Section 2 describes the datasets and methods. In
127 Section 3.1, the climatology and variability of surface pressure over the TP are
128 presented. In Section 3.2, the correlation between surface pressure bias and elevation
129 bias over the TP is analyzed and the corrections of surface pressure biases over the TP
130 are performed. Section 3.3 shows the trend of surface pressure after topography
131 correction over the TP. Section 3.4 analyzes the possible mechanism for surface
132 pressure changes over the TP. Section 4 summarizes the discussion and conclusions.

133 **2. Data and methods**

134 **2.1 Surface pressure from observation and multiple reanalyses**

135 Observed monthly surface pressure at 71 stations (**Figure 1**) is provided by the National
136 Meteorological Information Center, China Meteorological Administration
137 (NMIC/CMA). Stations are chosen according to selection procedures described in
138 previous papers [*You et al.*, 2008a; *You et al.*, 2008b]. Only stations above 2000 m were
139 selected. The period 1979-2013 is examined. We believe that the surface pressure at 71
140 stations is independent from the reanalysis products. In the future, such verifications
141 will become possible if all reanalysis producers publish the observations used along
142 with the reanalysis feedback.

143 Monthly surface pressures from five reanalyses are used, and more details are described
144 in **Table 1**. These include the National Centers for Environmental Prediction (NCEP)-

National Center for Atmospheric Research (NCAR) Reanalysis Project (NCEP1 hereafter) [*Kalnay et al.*, 1996; *Kistler et al.*, 2001]; the NCEP-Department of Energy (DOE) Reanalysis Project (NCEP2) [*Kanamitsu et al.*, 2002]; the European Centre for Medium-Range Weather Forecasts (ECMWF) Interim Reanalysis (ERA-Interim) [*Dee et al.*, 2011]; the Japan Meteorological Agency (JMA) 55 year Reanalysis Project (JRA55) [*Kobayashi et al.*, 2015]; and the National Aeronautics and Space Administration (NASA) Modern-Era Retrospective Analysis for Research and Applications (MERRA) [*Rienecker et al.*, 2011]. It should be noted that there are other reanalyses, but due to lack of time we could not consider them all. We hence decided to focus the work on a few widely-used reanalysis products, because they are well-documented. These products are known to contain limitations, and some products have been replaced by more recent products. For example, both NCEP1 and NCEP2, ERA-Interim, and MERRA were superseded by CFSR, ERA5 [*Hersbach et al.*, 2018], and MERRA-2 [*Gelaro et al.*, 2017], respectively. Reanalyses vary in terms of temporal range and horizontal resolution. Thus to eliminate differences due to contrasting resolutions, all reanalyses and observations were re-gridded to a 1°×1° horizontal grid for 1979-2013. Note that some products had a resolution higher than 1°×1° resolution, so the regridding operation induced additional errors for the comparison.

The reanalyses studied here use different models and assimilation methods, which can lead to differences in the datasets [*Bao and Zhang*, 2013; *Kang et al.*, 2010; *Ma et al.*, 2009; *Simmons et al.*, 2004; *Wang and Zeng*, 2012; *You et al.*, 2017]. Thus, the surface pressure and its trends over the TP may vary across the different reanalyses.To

167 determine how well the reanalyses perform over the TP, surface pressure fields from
168 each reanalysis are compared with the observed monthly surface pressure from the 71
169 stations.

170 **2.2 Observed elevation and model elevation**

171 To explain differences between observations and multiple reanalyses, a topographical
172 analysis is performed using the statistical methods followed by the previous papers [*You*
173 *et al.*, 2013b; *You et al.*, 2008b]. The observed elevation of each surface station is
174 provided by NMIC/CMA, and model elevations of each reanalysis (NCEP1, NCEP2,
175 ERA-Interim, MERRA and JRA55) can be obtained from its respective website [*Dee*
176 *et al.*, 2011; *Kalnay et al.*, 1996; *Kanamitsu et al.*, 2002; *Kistler et al.*, 2001; *Kobayashi*
177 *et al.*, 2015; *Rienecker et al.*, 2011]. All reanalyses are compared at the observations
178 locations. For this, we spatially interpolate all the reanalyses to the exact horizontal
179 position (and elevation) of the 71 surface stations and compare the trends and
180 climatology at the 71 stations rather than the grid points. We interpolate the reanalysis
181 data from the surrounding grid points to the site's location using bilinear interpolation,
182 and transform the grid surface pressure to the observation site's altitude using the
183 hydrostatic equation as in *You et al.* [2017]. The pressure from each reanalysis is
184 corrected to the observed station height assuming a linear lapse rate.

185 **2.3 Elevation correction methods**

186 The elevation correction at each station is described by:

$$P_2 = P_1[1 - \frac{\Gamma(z_2 - z_1)}{T_1}]^{\frac{g}{R_d\Gamma}} \quad (1)$$

where P_2 and P_1 are the corrected and original reanalysis surface pressures, Γ is the vertical temperature lapse rate, z_2 and z_1 are the model and station elevations, T_1 is the surface air temperature of each reanalysis dataset horizontally interpolated into the observation locations, R_d is the gas constant for dry air and g is the acceleration due to gravity. To calculate the Γ, the temperature profiles from sounding data and multiple reanalyses dataset over the TP on an annual and seasonal basis are plotted (**Figure 2**). Results indicate that the temperature profiles from the reanalyses are consistent with the observed profiles at the sounding stations over the TP. This suggests that the temperature from the reanalyses can be used to calculate the Γ. The detailed method is shown as follows: First, the pressure level of the lowest layer above the ground is denoted as P1, and 300hPa pressure level is denoted as P2. Meanwhile, both temperature (T) and geopotential height data (H) between level P1 and P2 are extracted, respectively. The Γ is calculated by linear regression based the following formula:

$$T = \Gamma H + b \quad (2)$$

Afterwards, the regression coefficient Γ of each station in each year is calculated. The annual and seasonal Γ from multiple reanalyses is summarized in **Table 2**.

To assess the success of this correction, the root-mean-square error (RMSE) is calculated after correction as:

$$\mathrm{RMSE} = \sqrt{\frac{1}{n}\sum_{i=1}^{i=n}(P - P_{obs})^2} \quad (3)$$

where P represents corrected surface pressure of each reanalysis in turn, P_{obs} is the corresponding station observation and N is the number of station sites.

209 **2.4 Diagnostic equation**

210 To investigate the possible mechanism of surface pressure anomalies and long-term
211 trend, the diagnostic equation is performed based on monthly products from ERA-
212 Interim reanalysis [*Dee et al.*, 2011]. Based on equation of static equilibrium, low-level
213 geopotential height can be calculated from Eq. (4):

214 $$\mathrm{z}_1 = \mathrm{z}_2 - R_d \int_{p_2}^{p_1} \frac{T_v}{g} \mathrm{dlnp} \quad (4)$$

215 where z_1 and z_2 are 600 hPa and 100 hPa geopotential height, respectively.

216 Virtual temperature (T_v) is given as:.

217 $$T_v = (1 +$$

218 $0.608q)T$, (5)

219 Interannual anomaly of each variable during 1979–2013 is:

220 $$\Delta\mathrm{A} = A - \bar{A} \quad (6)$$

221 where $\bar{A}$ is the climate mean states of a variable, $\Delta\mathrm{A}$ is the deviation or anomaly of a
222 variable from climate mean status.

223 Based on Eq. (6), the interannual anomaly form of Eq. (4) is:

224 $$\Delta\mathrm{z}_1 = \Delta\mathrm{z}_2 - R_d \int_{p_2}^{p_1} \frac{\Delta T_v}{gp} \mathrm{dp} \quad (7)$$

225 Where $\Delta\mathrm{z}_1$ and $\Delta\mathrm{z}_2$ is interannual anomaly of $\mathrm{z}_1$and z_2, respectively. ΔT_v is the
226 interannual anomaly of virtual temperature. Eq. (7) indicates that the interannual
227 anomaly of z_1 depends on both the interannual anomaly of z_2 and the atmospheric
228 column temperature. Furthermore, the anomaly of z_1 varies in-phase with the anomaly
229 of z_2, but it has the opposite phase with variation from the anomaly of atmospheric
230 column temperature.

231 Moreover, atmospheric column temperature is closely associated with atmosphere
232 diabatic heating. The interannual anomaly of diabatic heating ΔQ is balanced by the
233 interannual anomalies of latent heat release ΔLH, surface sensible heat ΔSH, and net
234 atmospheric radiation ΔRC.

235 $$\Delta Q = \Delta LH + \Delta RC + \Delta SH \quad (8)$$

236 Latent heat LH can be calculated from precipitation:

237 $$LH = L_w \rho_w P \quad (9)$$

238 Net atmospheric radiation RC can be calculated by the difference from net radiation
239 on the top of atmosphere (Rn_{toa}) and net radiation on the surface ground (Rn_{sfc}).

240 $$RC = Rn_{toa} - Rn_{sfc} \quad (10)$$

241 Finally, trends and s significance are estimated using the Mann-Kendall test and Sen's
242 slope estimates [*Sen*, 1968]. All time series are calculated at monthly resolution. A trend
243 is considered to be statistically significant if it is significant at the 5% level.

244 **3. Results**

245 **3.1 Climatology and variability of surface pressure over the TP**

246 **Table 3** summarizes annual and seasonal means and relative bias of surface pressure
247 from both station observations and the five reanalyses (NCEP1, NCEP2, ERA-Interim,
248 MERRA and JRA55) at monthly resolution during 1979–2013. Using station data, the
249 highest/lowest surface pressures occur in autumn/winter. All the reanalyses
250 underestimate the observations with the relative error between 3% and 6%. NCEP2 is
251 closest to the observations and MERRA appears to have the largest differences. The

252 spatial distribution of mean absolute biases (reanalysis minus observation) of surface
253 pressure is shown on an annual and seasonal basis in **Figure 3**. All reanalyses
254 underestimate station pressure, which is consistent with the previous study during 2002-
255 2004 [*Wang and Zeng*, 2012]. The largest absolute biases occur in the south of the
256 plateau and in areas such as the Sichuan basin, but there are also patches of large
257 negative bias in the north-west of the plateau. It is striking that all five of the reanalyses
258 show similar patterns, reaching over 100 hPa in the worst locations which tend to occur
259 in two latitudinal bands around 30°N and 36°N.

260 **3.2 Corrections of surface pressure biases from reanalyses over the TP**

261 All reanalyses underestimate the observed elevation, and much of the difference
262 between observed pressure and reanalysis data may be explained by topographical
263 errors. In most cases, elevation differences (model minus surface station elevation, ΔH)
264 are positive because surface stations are situated in flat areas and valley bottoms which
265 tend to be lower than the reanalysis model topography [*You et al.*, 2013b]. Stations over
266 the TP are predominantly in lower mountain valleys on the southern and eastern parts
267 of the plateau, surrounded by higher peaks (where people live). This would explain a
268 general underestimation of surface pressure in the reanalyses. The different spatial
269 resolution between stations (points) and reanalysis grids, coupled with intrinsic
270 topographic bias, can lead to large elevation differences and in part this elevation
271 difference causes the differences in the surface pressure. The underestimation of surface
272 pressure in all reanalyses is mainly explained by the overestimation of the elevation in

the model. This is consistent with previous studies [*Ma et al.*, 2009; *Ma et al.*, 2008; *You et al.*, 2013b; *You et al.*, 2008b] which found a cold bias of NCEP/NCAR and ERA-40 to be mainly a result of differences in topographical height, and secondly due to station aspect and slope gradient.

Because much of the surface pressure bias between observations and reanalyses is explained by elevation differences, it is vital to remove this [*Kang et al.*, 2010; *Ma et al.*, 2009; *Ma et al.*, 2008; *Song et al.*, 2016; *Xie et al.*, 2014; *You et al.*, 2013b; *You et al.*, 2017; *Zhao et al.*, 2008]. Thus, the interpolated surface pressure was corrected for each reanalysis separately using the topographic correction. The spatial distribution of mean absolute bias (corrected reanalyses minus observation) is shown in **Figure 4**. The percentage of improvement after corrections is summarized in the bottom rows of **Table 4**. Dramatic improvements are achieved through elevation correction and differences of all reanalysis datasets are reduced by more than 90%. The best results are ERA-Interim and MERRA whose difference is reduced by more than 95%, closely followed by JRA55. The success of elevation correction for temperature showed seasonal and regional dependency [*Zhao et al.*, 2008], and is slightly better in summer than in winter. This is unsurprising since the vertical structure of the atmosphere is typically more well-mixed and uniform in summer, and inversions are less frequent (which would invalidate a simple correction) [*Pepin et al.*, 2011; *You et al.*, 2017]. For surface pressure, the effects of the correction also show seasonal dependence, and the remaining bias after correction does show some spatial variance. The bias for MERRA (which remains relatively large) is more than 30 hPa in southern parts of the TP but less

than 4 hPa in central areas. Most regions show relatively small biases between -5~10 hPa for NCEP1, NCEP2, ERA-Interim and JRA55. The complexity of the terrain, especially towards the southern edge of the plateau, is probably responsible for some of the remaining bias, consistent with past studies on temperature [*Zhao et al.*, 2008].

3.4 Trend of surface pressure after correction over the TP

Figure 5 and **Figure 6** show the regional anomaly and spatial trends of surface pressure from observations and reanalyses after correction considering the elevation difference over the TP on an annual and seasonal basis. **Table 5** summarizes the annual and seasonal means and trends of surface pressure from observation and multiple reanalyses after elevation bias correction. On an annual basis, mean regional surface pressure series from both observations and reanalyses increase slowly until the mid-2000s but then show a significant decrease afterwards (**Figure 5**). It is also clear that all reanalyses are strongly correlated with the station data, indicating that they can clearly reproduce decadal variation in surface pressure. Over the whole period, the trends of surface pressure are insignificant from all sources. Examining spatial patterns in more detail, the majority of individual stations shows a decrease in surface pressure. During 1979-2013, it is clear most stations in the central/northern regions show significant negative trends on an annual basis (**Figure 6** top left panel). Stations in the central and northern TP tend to have larger trend magnitudes, which correspond with downward trends in total cloud cover and surface relative humidity in the region [*You et al.*, 2015b]. However, reanalyses tend to show increases in pressure over the same period,

316 particularly NCEP1 and MERRA. On a seasonal basis, the trends over the whole period
317 from observations and reanalyses also show large differences. The maps show areas of
318 significant trend change, and both observations and reanalyses show largest increases
319 in spring. The other seasons have smaller trend values which in most regions are
320 insignificant. As was the case for annual trends, the observations again show more
321 negative trends in general than reanalyses in most seasons.

322 **3.4 Possible mechanism influencing surface pressure over the TP**

323 To investigate possible mechanisms that influence surface pressure over the TP,
324 especially in spring, an atmospheric diagnosis is performed based on ERA-Interim
325 reanalysis. **Figure 7** shows the time series of surface pressure anomalies, 100 hPa and
326 600 hPa geopotential height, and column temperature over the TP during 1979–2013.
327 **Table 6** summarizes the correlation coefficients among these variables in spring. It is
328 clear that the surface pressure over the TP is positively correlated with the 100hPa and
329 600hPa geopotential height, with correlation coefficients of 0.4 and 0.97, respectively.
330 Thus, the changes of surface pressure over the TP can be inferred from the 600 hPa
331 geopotential height. Meanwhile, the surface pressure over the TP has similar
332 interannual variabilities with 100hPa and 600hPa geopotential height, indicating the
333 quasi-barotropic atmospheric structure over the TP.

334 From equations (4-8) in the methods, the changes of 600hPa geopotential height are
335 determined by 100 hPa geopotential height and atmospheric column temperature, then
336 indirectly influence the surface pressure over the TP. Moreover, the atmospheric

337 column temperature is influenced by diabatic heating, which is balanced by latent heat,
338 surface sensible heat and atmospheric net radiation, respectively. **Figure 8** and **Figure**
339 **9** show the time series and spatial trends of standardized column temperature, diabatic
340 heating, latent heat, surface sensible heat, and net atmospheric radiation over the TP
341 during 1979–2013 on an annual and seasonal basis based on ERA-Interim reanalysis.
342 Their correlation coefficients are summarized in **Table 7**. The column temperature has
343 negative correlations with both surface sensible heat and net atmospheric radiation, and
344 positive correlations with diabatic heating and latent heat, and all the correlation
345 coefficients pass the significance test (**Table 7**). In **Figure 9**, it is clear that decreasing
346 sensible heat increases the heat flux transformation from ground to the bottom air, and
347 increasing latent heat leads to the endothermic increases, as well as the decreasing net
348 atmospheric radiation results to the energy transferring from atmosphere to surface.
349 These changes contribute to the decreasing diabatic heating, causing the increase of
350 atmospheric column temperature, which is consistent with the increasing column
351 temperature over the TP (**Figure 10**). Thus, this suggests that the significant increase of
352 both 100 hPa geopotential height and column temperature over the TP mainly accounts
353 for the significant increase of surface pressure over the TP.

354 **4. Discussion and Conclusions**

355 In this study, the variability and reliability of surface pressure over the TP are analyzed
356 from station observations and multiple reanalyses during 1979-2013. This is the first
357 time that such analyses have been performed at high elevations and this is an important

finding, given that mountain station pressure can be regarded as an indicator of climate change [*Toumi et al.*, 1999]. This suggests that the vertical expansion/warming of the atmosphere at high elevations will not necessarily lead to increased pressure at high elevation stations. The physical relationship between the surface temperature and pressure reflects the changing nature of the seasonal snow cover (land surface property) and cloud in the region [*You et al.*, 2017]. Meanwhile, the finding that all reanalyses underestimate surface pressure over the TP is consistent with other studies. Recent work in East Antarctica shows reanalyses explain more than 87% of the average variance of surface pressure shown by observations during 2005-2008 [*Xie et al.*, 2014]. Despite discrepancies between observations and reanalyses, inter-annual correlations between the two were high. Similar results were also shown over the Southern Ocean and Antarctica [*Hines et al.*, 2000] since the 1980s. Thus our finding that surface pressure from reanalyses (NCEP1, NCEP2, ERA-Interim, MERRA and JRA55) over the TP is broadly similar to surface pressure from observations and that reanalyses can capture the decadal variability of pressure is supported by analyses elsewhere.

Analysis of pressure trends in this study reveals a significant decrease of surface pressure after the mid-2000s in both observations and all reanalyses. In this study, it is found that the increases in both 100 hPa geopotential height and column temperature over the TP result in increases in 600 hPa geopotential height, which likely account for the significant increase of surface pressure in spring over the TP (**Figure 11**). However, there is little variation in temperature lapse rate with season, with the highest temperature lapse rate in spring. The surface pressure change is not related to the change

of temperature lapse rate, but is associated with the altitude difference with larger trend magnitude. A scaling of the vertical equation of motion shows on monthly time scales the vertical motion is negligible. The elevation biases extrapolated to the stations is accurately given, and the effect of vertical interpolation will be helpful through using hydrostatic equation. Thus, pressure increase is most evident in spring, which doesn't depend on the value of the temperature lapse rate but on the thermal condition change over the TP.

There are significant negative correlations between surface pressure bias and elevation bias (reanalysis minus observation) on both an annual and seasonal basis, suggesting that elevation difference is the main reason for the surface pressure biases. This phenomenon has also been revealed for surface air temperature over the TP [*You et al.*, 2013b] and in eastern China [*Zhao et al.*, 2008]. Therefore, topographical correction is essential before other analyses are conducted, and most of the bias can be eliminated through topographical correction. ERA-Interim, MERRA and JRA55 perform best after the elevation correction and the percentage of improvement after correction is more than 95%, while NCEP1 and NCEP2 perform the second-best in interpolation considering elevation difference with the percentage of improvement after correction of 94% (**Table 4**). The better performance of ERA-Interim, MERRA and JRA55 is probably due to the forecast model, the observation handling, operational weather forecasting and assimilation methods [*Dee et al.*, 2011; *Rienecker et al.*, 2011; *Simmons et al.*, 2004]. After correction there are still biases in some of the more pronounced basins (e.g. Qaidam basin) and on the southern edges of the plateau where the

topography is particularly complex. Most of the surface stations in the TP are located in the central and eastern parts of the TP, and therefore their topographic slope or station orientation could influence the trend magnitudes of pressure over the TP to a certain degree [*You et al.*, 2013b]. Future work must therefore go beyond elevational differences and consider topographical factors such as slope aspect, exposure (convexity and concavity) and their influences on explaining remaining bias. This can further reduce uncertainty caused by the complex topography [*Moore*, 2012; *Toumi et al.*, 1999; *Trenberth et al.*, 1987]. Reanalyses can be used to extend surface pressure trend analysis to the western TP where there are few stations, but it is critical to calibrate the reanalyses against station observations where they exist, which in turn will require a more detailed understanding of topographic factors on model bias [*You et al.*, 2013b; *You et al.*, 2017; *You et al.*, 2008a]. This requires that reanalyses release the observations they used, so that one can verify that the calibration observations are independent from reanalysis.

Acknowledgments. This study is supported by National Key R&D Program of China (2016YFA0601702) and National Natural Science Foundation of China (41771069). NCEP Reanalysis data are provided by the NOAA/OAR/ESRL PSD, Boulder, Colorado, USA, from their Web site at https://www.esrl.noaa.gov/psd/. We are very grateful to the reviewers for their constructive comments and thoughtful suggestions.

References

Allan, R., and T. Ansell (2006), A New Globally Complete Monthly Historical Gridded Mean Sea Level Pressure Dataset (HadSLP2): 1850–2004, *Journal of Climate*, *19*(22),

5816-5842, doi:10.1175/JCLI3937.1.

Bao, X., and F. Zhang (2013), Evaluation of NCEP–CFSR, NCEP–NCAR, ERA-Interim, and ERA-40 reanalysis datasets against independent sounding observations over the Tibetan Plateau, *Journal of Climate*, *26*(1), 206-214.

Barnett, T. P., J. C. Adam, and D. P. Lettenmaier (2005), Potential impacts of a warming climate on water availability in snow-dominated regions, *Nature*, *438*(7066), 303-309, doi:10.1038/nature04141.

Cai, D., Q. You, K. Fraedrich, and Y. Guan (2017), Spatiotemporal Temperature Variability over the Tibetan Plateau: Altitudinal Dependence Associated with the Global Warming Hiatus, *Journal of Climate*, *30*, 969-984, doi:10.1175/jcli-d-16-0343.1.

Chen, T. C., J. M. Chen, S. Schubert, and L. L. Takacs (1997), Seasonal variation of global surface pressure and water vapor, *Tellus A*, *49*, 613-621.

Compo, G. P., J. S. Whitaker, and P. D. Sardeshmukh (2006), Feasibility of a 100-Year Reanalysis Using Only Surface Pressure Data, *Bulletin of the American Meteorological Society*(87), 175-190.

Cullather, R., and A. Lynch (2003), The annual cycle and interannual variability of atmospheric pressure in the vicinity of the North Pole, *International Journal of Climatology*, *23*(10), 1161-1183.

Cuo, L., Y. Zhang, Q. Wang, L. Zhang, B. Zhou, Z. Hao, and F. Su (2013), Climate Change on the Northern Tibetan Plateau during 1957-2009: Spatial Patterns and Possible Mechanisms, *Journal of Climate*, *26*(1), 85-109, doi:10.1175/jcli-d-11-00738.1.

Dee, D. P., et al. (2011), The ERA-Interim reanalysis: configuration and performance of the data assimilation system, *Quarterly Journal of the Royal Meteorological Society*, *137*(656), 553-597, doi:10.1002/qj.828.

Duan, A. M., G. Wu, Y. Liu, Y. Ma, and P. Zhao (2012), Weather and climate effects of the Tibetan Plateau, *Advances in Atmospheric Sciences*, *29*(5), 978-992, doi:10.1007/s00376-012-1220-y.

Duan, A. M., and G. X. Wu (2005), Role of the Tibetan Plateau thermal forcing in the summer climate patterns over subtropical Asia, *Climate Dynamics*, *24*(7-8), 793-807,

454 doi:10.1007/s00382-004-0488-8.
455 Fu, R., Y. Hu, J. S. Wright, J. H. Jiang, R. E. Dickinson, M. Chen, M. Filipiak, W. G.
456 Read, J. W. Waters, and D. L. Wu (2006), Short circuit of water vapor and polluted air
457 to the global stratosphere by convective transport over the Tibetan Plateau, *Proceedings*
458 *of the National Academy of Sciences*, *103*(15), 5664-5669.
459 Gelaro, R., et al. (2017), The Modern-Era Retrospective Analysis for Research and
460 Applications, Version 2 (MERRA-2), *Journal of Climate*, *30*(14), 5419-5454,
461 doi:10.1175/JCLI-D-16-0758.1.
462 Gillett, N. P., F. W. Zwiers, A. J. Weaver, and P. Stott (2003), Detection of human
463 influence on sea-level pressure, *Nature*, *422*, 292-294.
464 Hahn, D. G., and J. Shukla (1976), An Apparent Relationship between Eurasian Snow
465 Cover and Indian Monsoon Rainfall, *Journal of the Atmospheric Sciences*, *33*(12),
466 2461-2462, doi:10.1175/1520-0469(1976)033<2461:AARBES>2.0.CO;2.
467 Han, W., et al. (2010), Patterns of Indian Ocean sea-level change in a warming climate,
468 *Nature Geosci*, *3*(8), 546-550.
469 Hersbach, H., P. de Rosnay, B. Bell, D. Schepers, A. Simmons, C. Soci, S. Abdalla, M.
470 Alonso-Balmaseda, and G. B. Balsamo, P.; (2018), Operational global reanalysis:
471 Progress, future directions and synergies with NWP, *ERA Report Series 27, ECMWF,*
472 *Shinfield Park, Reading, United Kingdom*.
473 Hines, K. M., D. H. Bromwich, and G. J. Marshall (2000), Artificial Surface Pressure
474 Trends in the NCEP–NCAR Reanalysis over the Southern Ocean and Antarctica,
475 *Journal of Climate*, *13*(22), 3940-3952.
476 Ingleby, B. (2015), Global assimilation of air temperature, humidity, wind and pressure
477 from surface stations, *Quarterly Journal of the Royal Meteorological Society*, *141*(687),
478 504-517, doi:doi:10.1002/qj.2372.
479 Jacques, A. A., J. D. Horel, E. T. Crosman, and F. L. Vernon (2015), Central and Eastern
480 U.S. Surface Pressure Variations Derived from the USArray Network, *Monthly Weather*
481 *Review*, *143*(4), 1472-1493, doi:10.1175/MWR-D-14-00274.1.
482 Kalnay, E., et al. (1996), The NCEP/NCAR 40-year reanalysis project, *Bulletin of the*
483 *American Meteorological Society*, *77*(3), 437-471.

484 Kanamitsu, M., W. Ebisuzaki, J. Woollen, S. K. Yang, J. J. Hnilo, M. Fiorino, and G. L.
485 Potter (2002), NCEP-DOE AMIP-II reanalysis (R-2), *Bulletin of the American*
486 *Meteorological Society*, *83*(11), 1631-1643, doi:10.1175/bams-83-11-1631.
487 Kang, S. C., Y. W. Xu, Q. L. You, W. A. Flugel, N. Pepin, and T. D. Yao (2010), Review
488 of climate and cryospheric change in the Tibetan Plateau, *Environmental Research*
489 *Letters*, *5*(1), 015101, doi:10.1088/1748-9326/5/1/015101.
490 Kistler, R., et al. (2001), The NCEP-NCAR 50-year reanalysis: Monthly means CD-
491 ROM and documentation, *Bulletin of the American Meteorological Society*, *82*(2), 247-
492 267.
493 Kobayashi, S., et al. (2015), The JRA-55 Reanalysis: General specifications and basic
494 characteristics, *J. Meteor. Soc. Japan*, *93*, 5-48.
495 Koppel, L. L., L. F. Bosart, and D. Keyser (2000), A 25-yr Climatology of Large-
496 Amplitude Hourly Surface Pressure Changes over the Conterminous United States,
497 *Monthly Weather Review*, *128*(1), 51-68.
498 Liu, X., Z. Cheng, L. Yan, and Z.-Y. Yin (2009), Elevation dependency of recent and
499 future minimum surface air temperature trends in the Tibetan Plateau and its
500 surroundings, *Global and Planetary Change*, *68*(3), 164-174.
501 Ma, L. J., T. Zhang, O. W. Frauenfeld, B. S. Ye, D. Q. Yang, and D. H. Qin (2009),
502 Evaluation of precipitation from the ERA-40, NCEP-1, and NCEP-2 Reanalyses and
503 CMAP-1, CMAP-2, and GPCP-2 with ground-based measurements in China, *Journal*
504 *of Geophysical Research-Atmospheres*, *114*, D09105.
505 Ma, L. J., T. J. Zhang, Q. X. Li, O. W. Frauenfeld, and D. H. Qin (2008), Evaluation of
506 ERA-40, NCEP-1, and NCEP-2 reanalysis air temperatures with ground-based
507 measurements in China, *Journal of Geophysical Research-Atmospheres*, *113*, D15115,
508 doi:10.1029/2007jd009549.
509 Mass, C. F., and L. E. Madaus (2014), Surface Pressure Observations from
510 Smartphones: A Potential Revolution for High-Resolution Weather Prediction?,
511 *Bulletin of the American Meteorological Society*, *95*(9), 1343-1349.
512 Moore, G. (2012), Surface pressure record of Tibetan Plateau warming since the 1870s,
513 *Quarterly Journal of the Royal Meteorological Society*, *138*(669), 1999-2008.

514 Pepin, N. C., C. Daly, and J. Lundquist (2011), The influence of surface versus free-air
515 decoupling on temperature trend patterns in the western United States, *Journal of*
516 *Geophysical Research-Atmospheres*, *116*, D10109, doi:10.1029/2010jd014769.
517 Rangwala, I., J. Miller, G. Russell, and M. Xu (2010), Using a global climate model to
518 evaluate the influences of water vapor, snow cover and atmospheric aerosol on warming
519 in the Tibetan Plateau during the twenty-first century, *Climate Dynamics*, *34(6)*, 859-
520 872.
521 Rienecker, M. M., et al. (2011), MERRA: NASA's Modern-Era Retrospective Analysis
522 for Research and Applications, *Journal of Climate*, *24*(14), 3624-3648,
523 doi:10.1175/jcli-d-11-00015.1.
524 Saha, K., H. van den Dool, and S. Saha (1994), On the Annual Cycle in Surface Pressure
525 on the Tibetan Plateau Compared to Its Surroundings, *Journal of Climate*, *7*(12), 2014-
526 2019.
527 Sen, P. K. (1968), Estimates of regression coefficient based on Kendall's tau, *Journal*
528 *of the American Statistical Association*, *63*, 1379-1389.
529 Simmons, A. J., P. D. Jones, V. D. Bechtold, A. C. M. Beljaars, P. W. Kallberg, S.
530 Saarinen, S. M. Uppala, P. Viterbo, and N. Wedi (2004), Comparison of trends and low-
531 frequency variability in CRU, ERA-40, and NCEP/NCAR analyses of surface air
532 temperature, *Journal of Geophysical Research-Atmospheres*, *109*, D24115
533 doi:10.1029/2004jd005306.
534 Song, C. Q., L. H. Ke, K. S. Richards, and Y. Z. Gui (2016), Homogenization of surface
535 temperature data in High Mountain Asia through comparison of reanalysis data and
536 station observations, *International Journal of Climatology*, *36*, 1088-1101.
537 Toumi, R., N. Hartell, and K. Bignell (1999), Mountain station pressure as an indicator
538 of climate change, *Geophys. Res. Lett.*, *26*(12), 1751-1754.
539 Trenberth, K. E. (1981), Seasonal variations in global sea level pressure and the total
540 mass of the atmosphere, *Journal of Geophysical Research: Atmospheres*, *86*, 5236-
541 5246.
542 Trenberth, K. E., J. R. Christy, and J. G. Olson (1987), Global atmospheric mass,
543 surface pressure, and water vapor variations, *Journal of Geophysical Research:*

544 *Atmospheres*, *92*, 14815-14826.
545 van den Dool, H. M., and S. Saha (1993), Seasonal Redistribution and Conservation of
546 Atmospheric Mass in a General Circulation Model, *Journal of Climate*, *6*(1), 22-30,
547 doi:10.1175/1520-0442(1993)006<0022:SRACOA>2.0.CO;2.
548 Van Wijngaarden, W. (2005), Examination of trends in hourly surface pressure in
549 Canada during 1953-2003, *Int. J. Climatol.*, *25*(15), 2041-2049.
550 Wang, A., and X. Zeng (2012), Evaluation of multireanalysis products with in situ
551 observations over the Tibetan Plateau, *Journal of Geophysical Research: Atmospheres*
552 *(1984–2012)*, *117*(D5), D05102.
553 Wheatley, D., and D. Stensrud (2010), The impact of assimilating surface pressure
554 observations on severe weather events in a WRF mesoscale ensemble system, *Monthly*
555 *weather review*, *138*, 1673-1694.
556 Wu, G. X., A. M. Duan, Y. M. Liu, J. Mao, R. Ren, Q. Bao, B. He, B. Liu, and W. Hu
557 (2015), Tibetan Plateau climate dynamics: recent research progress and outlook,
558 *National Science Review*, *2*, 100-116.
559 Wu, T. W., and Z. A. Qian (2003), The relation between the Tibetan winter snow and
560 the Asian summer monsoon and rainfall: An observational investigation, *Journal of*
561 *Climate*, *16*(12), 2038-2051.
562 Xie, A. H., I. Allison, C. D. Xiao, S. M. Wang, J. W. Ren, and D. H. Qin (2014),
563 Assessment of Surface Pressure between Zhongshan and Dome a in East Antarctica
564 from Different Meteorological Reanalyses, *Arctic, Antarctic, and Alpine Research*, *46*,
565 669-681.
566 Yanai, M. H., and C. Li (1994), Mechanism of Heating and the Boundary Layer over
567 the Tibetan Plateau, *Monthly weather review*, *122*, 305-323.
568 Yanai, M. H., C. Li, and Z. Song (1992), Seasonal heating of the Tibetan Plateau and
569 its effects on the evolution of the Asian summer monsoon, *Journal of the*
570 *Meteorological Society of Japan 70*, 319-351.
571 Yang, K., H. Wu, J. Qin, C. Lin, W. Tang, and Y. Chen (2014), Recent climate changes
572 over the Tibetan Plateau and their impacts on energy and water cycle: A review, *Global*
573 *and Planetary Change*, *112*, 79-91.

574 Yang, K., B. S. Ye, D. G. Zhou, B. Y. Wu, T. Foken, J. Qin, and Z. Y. Zhou (2011),
575 Response of hydrological cycle to recent climate changes in the Tibetan Plateau,
576 *Climatic Change*, *109*(3-4), 517-534, doi:10.1007/s10584-011-0099-4.
577 You, Q. L., K. Fraedrich, J. Min, S. Kang, X. Zhu, G. Ren, and X. Meng (2013a), Can
578 temperature extremes in China be calculated from reanalysis?, *Global and Planetary*
579 *Change*, *111*, 268-279.
580 You, Q. L., K. Fraedrich, G. Ren, N. Pepin, and S. Kang (2013b), Variability of
581 temperature in the Tibetan Plateau based on homogenized surface stations and
582 reanalysis data, *International Journal of Climatology*, *33*(6), 1337-1347.
583 You, Q. L., Z. H. Jiang, G. Moore, Y. T. Bao, L. Kong, and S. C. Kang (2017), Revisiting
584 the relationship between observed warming and surface pressure in the Tibetan Plateau,
585 *Journal of Climate*, *30*, 1721-1737.
586 You, Q. L., S. C. Kang, E. Aguilar, and Y. P. Yan (2008a), Changes in daily climate
587 extremes in the eastern and central Tibetan Plateau during 1961-2005, *Journal of*
588 *Geophysical Research-Atmospheres*, *113*, D07101.
589 You, Q. L., S. C. Kang, N. Pepin, and Y. P. Yan (2008b), Relationship between trends
590 in temperature extremes and elevation in the eastern and central Tibetan Plateau, 1961-
591 2005, *Geophys. Res. Lett.*, *35*, L04704, doi:10.1029/2007gl032669.
592 You, Q. L., J. Min, W. Zhang, N. Pepin, and S. Kang (2015a), Comparison of multiple
593 datasets with gridded precipitation observations over the Tibetan Plateau, *Climate*
594 *Dynamics*, *45*(3), 791-806, doi:10.1007/s00382-014-2310-6.
595 You, Q. L., J. Z. Min, H. B. Lin, S. Kang, and P. Nick (2015b), Observed climatology
596 and trend in relative humidity in the eastern and central Tibetan Plateau, *Journal of*
597 *Geophysical Research: Atmospheres*, *120*, 3610-3621.
598 You, Q. L., A. Sanchez-Lorenzo, M. Wild, D. Folini, K. Fraedrich, G. Ren, and S. Kang
599 (2013c), Decadal variation of surface solar radiation in the Tibetan Plateau from
600 observations, reanalysis and model simulations, *Climate Dynamics*, *40*(7-8), 2073-2086.
601 Zhao, T., W. Guo, and C. Fu (2008), Calibrating and evaluating reanalysis surface
602 temperature error by topographic correction, *Journal of Climate*, *21*(6), 1440-1446,
603 doi:10.1175/2007jcli1463.1.

Zishka, K. M., and P. J. Smith (1980), The Climatology of Cyclones and Anticyclones over North America and Surrounding Ocean Environs for January and July, 1950–77, *Monthly weather review*, *108*, 387-401.

634 **Table 1.** Summary of the observations and multiple reanalyses used in this study.

Name	Organization	Temporal resolution	Horizontal resolution	Assimilation methods	Sources	References
NCEP1	NCEP/NCAR	1948-present	2.5°×2.5°	3D-VAR	http://www.esrl.noaa.gov	[*Kalnay et al.*, 1996]
NCEP2	NCEP/DOE	1979-present	2.5°×2.5°	3D-VAR	http://www.esrl.noaa.gov	[*Kanamitsu et al.*, 2002]
ERA-Interim	ECMWF	1979-present	0.5°×0.5°	4D-VAR	http://www.ecmwf.int	[*Dee et al.*, 2011]
MERRA	NASA GMAO	1979-present	0.5°×0.5°	3D-VAR, with incremental update	http://disc.sci.gsfc.nasa.gov	[*Rienecker et al.*, 2011]
JRA55	JMA	1958-present	1.25°×1.25°	4D-VAR	http://jra.kishou.go.jp	[*Kobayashi et al.*, 2015]

635

636

637

638

639

640

641

642

643

644

645

646

647

648

649 **Table 2**. Temperature lapse rate from multiple reanalyses datasets over the Tibetan

650 Plateau on an annual and seasonal basis, and the unit is °C/100m.

651

	Annual	Spring	Summer	Autumn	Winter
NCEP1	-0.66	-0.70	-0.64	-0.64	-0.65
NCEP2	-0.68	-0.73	-0.64	-0.67	-0.69
ERA-Interim	-0.68	-0.73	-0.62	-0.67	-0.72
MERRA	-0.69	-0.74	-0.62	-0.68	-0.73
JRA55	-0.67	-0.73	-0.62	-0.66	-0.69

652

653

654

655

656

657

658

659

660

661

662

663

664

665

666

667

668

669 **Table 3**. Annual and seasonal mean and relative bias of surface pressure from station
670 observations and multiple reanalyses (NCEP1, NCEP2, ERA-Interim, MERRA and
671 JRA55) over the Tibetan Plateau during 1979-2013. The relative bias is defined
672 as $\frac{\boldsymbol{Reanalysis-Observation}}{\boldsymbol{Observation}} \times 100\%$.
673

	Annual	Spring	Summer	Autumn	Winter
Mean (hPa)					
Observation	682.4	681.2	683.0	685.2	680.3
NCEP1	652.4	651.3	653.8	655.1	649.5
NCEP2	658.8	657.7	660.1	661.5	656.0
ERA-Interim	644.8	643.7	646.1	647.5	641.9
MERRA	643.4	642.4	644.9	646.0	640.4
JRA55	645.8	644.7	647.4	648.5	642.6
Relative bias (%)					
NCEP1	-4.4%	-4.4%	-4.3%	-4.4%	-4.5%
NCEP2	-3.5%	-3.5%	-3.4%	-3.5%	-3.6%
ERA-Interim	-5.5%	-5.5%	-5.4%	-5.5%	-5.6%
MERRA	-5.7%	-5.7%	-5.6%	-5.7%	-5.9%
JRA55	-5.4%	-5.4%	-5.2%	-5.4%	-5.5%

674
675
676
677
678
679
680
681
682
683
684
685

686 **Table 4**. Root mean square error of reanalyses surface pressure (reanalyses vs
687 observations) for horizontal bilinear interpolation and correction considering the
688 elevation difference on an annual and seasonal basis. The percentage reduction in bias
689 after correction is listed.

		Annual	Spring	Summer	Autumn	Winter
Horizontal bilinear interpolation	NCEP1	57.5	57.4	55.9	57.6	59.1
	NCEP2	54.7	54.6	53.1	54.8	56.2
	ERA Interim	56.2	56.1	54.9	56.3	57.6
	MERRA	57.8	57.6	56.3	58.0	59.3
	JRA55	55.6	55.5	54.1	55.8	57.2
Interpolation considering elevation difference	NCEP1	3.7	3.7	3.3	3.7	4.2
	NCEP2	3.0	3.0	2.9	3.0	3.3
	ERA-Interim	2.2	2.2	2.1	2.2	2.4
	MERRA	2.2	2.2	2.1	2.2	2.4
	JRA55	2.6	2.5	2.5	2.5	2.7
Percentage of improvement after correction	NCEP1	93.6%	93.6%	94.1%	93.7%	92.8%
	NCEP2	94.5%	94.5%	94.5%	94.5%	94.1%
	ERA-Interim	96.2%	96.1%	96.2%	96.1%	96.0%
	MERRA	96.2%	96.2%	96.3%	96.2%	96.0%
	JRA55	95.4%	95.4%	95.4%	95.4%	95.2%

690
691
692
693
694
695
696
697
698

699 **Table 5**. Annual and seasonal mean and trend of surface pressure from station
700 observations and multiple reanalyses (NCEP1, NCEP2, ERA-Interim, MERRA and
701 JRA55) after correction considering the elevation difference over the Tibetan Plateau
702 during 1979-2013.
703

		Annual	Spring	Summer	Autumn	Winter
Mean (hPa)						
Observation		682.4	681.2	683.0	685.2	680.3
NCEP1		684.7	683.5	684.8	687.5	683.1
NCEP2		684.1	682.8	684.5	686.9	682.2
ERA-Interim		682.8	681.6	683.1	685.7	681.0
MERRA		685.1	683.9	685.4	687.8	683.2
JRA55		683.7	682.4	684.2	686.5	681.6
Trend (hPa/decade)						
1979-2013	Observation	-0.04	**0.21**	-0.06	-0.13	-0.23
	NCEP1	0.06	**0.33**	0.02	-0.02	-0.05
	NCEP2	0.06	**0.35**	-0.01	0.01	-0.02
	ERA Interim	0.02	**0.27**	0.02	-0.03	-0.15
	MERRA	0.07	**0.30**	0.05	0.01	-0.11
	JRA55	-0.02	**0.23**	-0.06	-0.11	-0.18

704
705
706
707
708
709
710
711
712

713 **Table 6.** Correlation coefficients among surface pressure, 100 hPa geopotential height,
714 600 hPa geopotential height, and column air temperature based on ERA-Interim dataset
715 over the Tibetan Plateau in spring during 1979-2013. The single and double asterisks
716 indicate the value passed the 0.1 and 0.05 significant level, respectively.

Correlation coefficient	Surface pressure	100hPa geopotential height	600hPa geopotential height	Column temperature
Surface pressure	1	-	-	-
100hPa geopotential height	0.40**	1	-	-
600hPa geopotential height	0.97**	0.50**	1	-
Column temperature	0.16	0.96**	0.26	1

717
718
719
720
721
722
723
724
725
726
727
728
729

730

731 **Table 7.** Correlation coefficients between column temperature and diabatic heating, air

732 latent heat, surface sensible heat, as well as net atmospheric radiation based on ERA-

733 Interim dataset over the Tibetan Plateau in spring during 1979-2013. The single and

734 double asterisks indicate the value passed the 0.1 and 0.05 significant level, respectively.

	Diabatic heating	Air latent heat	Surface sensible heat	Net atmospheric radiation
Correlation coefficient	-0.36*	0.51**	-0.67**	0.43**

735

736

737

738

739

740

741

742

743

744

745

746

747

748

749

750

751 **Figure**

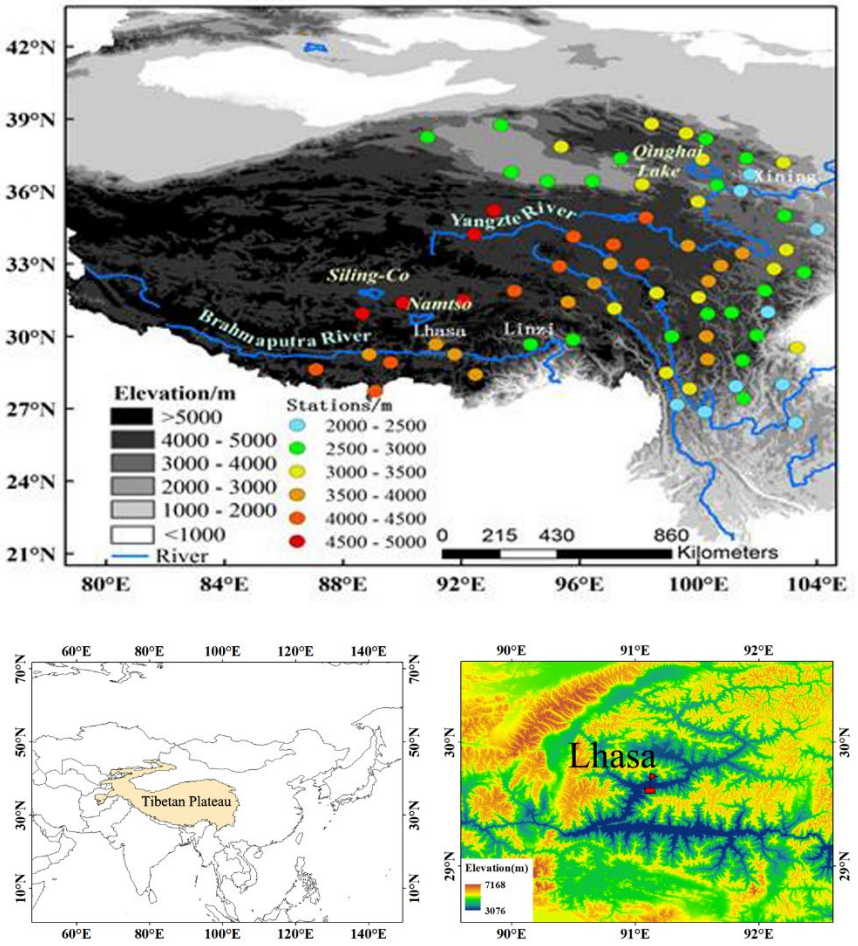

752

753 **Figure 1**. The distribution of 71 stations with elevation information over the Tibetan
754 Plateau. Most stations over the Tibetan Plateau are situated predominantly in flat areas
755 and lower mountain valleys on the southern and eastern parts of the Tibetan Plateau.
756 Lhasa station is shown as an example.

757

758

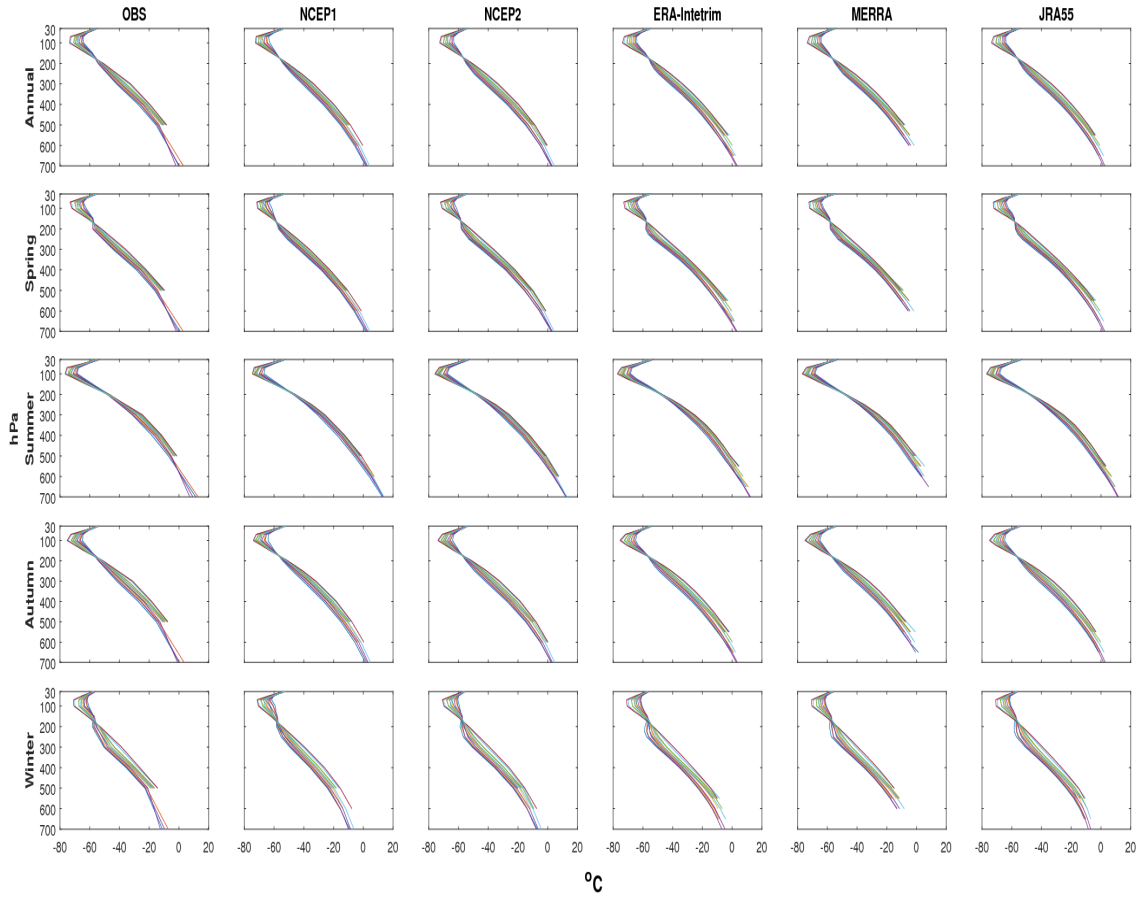

759

760 **Figure 2**. Temperature profile from 13 sounding stations and multiple reanalyses over

761 the Tibetan Plateau on an annual and seasonal basis. Each curve within a single panel

762 represents temperature profile from each sounding station and reanalysis.

763

764

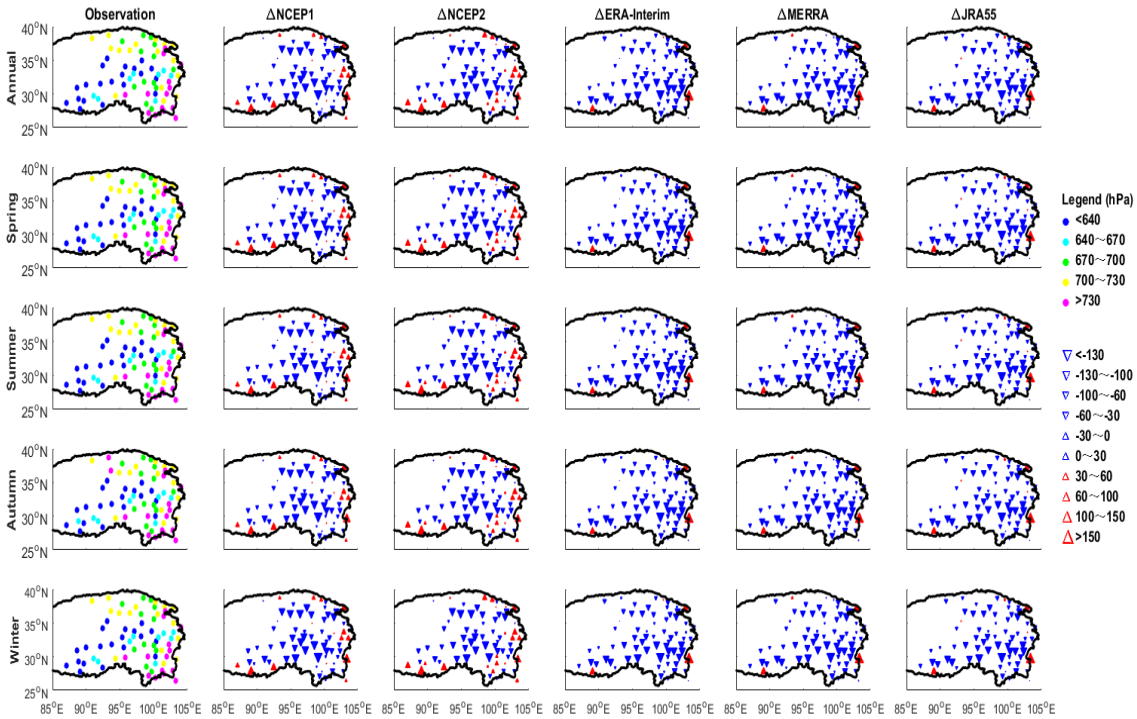

765

766 **Figure 3**. Spatial distribution of climatological surface pressure (top left) and difference

767 (Δ) between observation and five reanalyses (NCEP1, NCEP2, ERA-Interim, MERRA

768 and JRA55) before correction considering the elevation difference over the Tibetan

769 Plateau on an annual and seasonal basis. The unit is hPa.

770

771

772

773

774

775

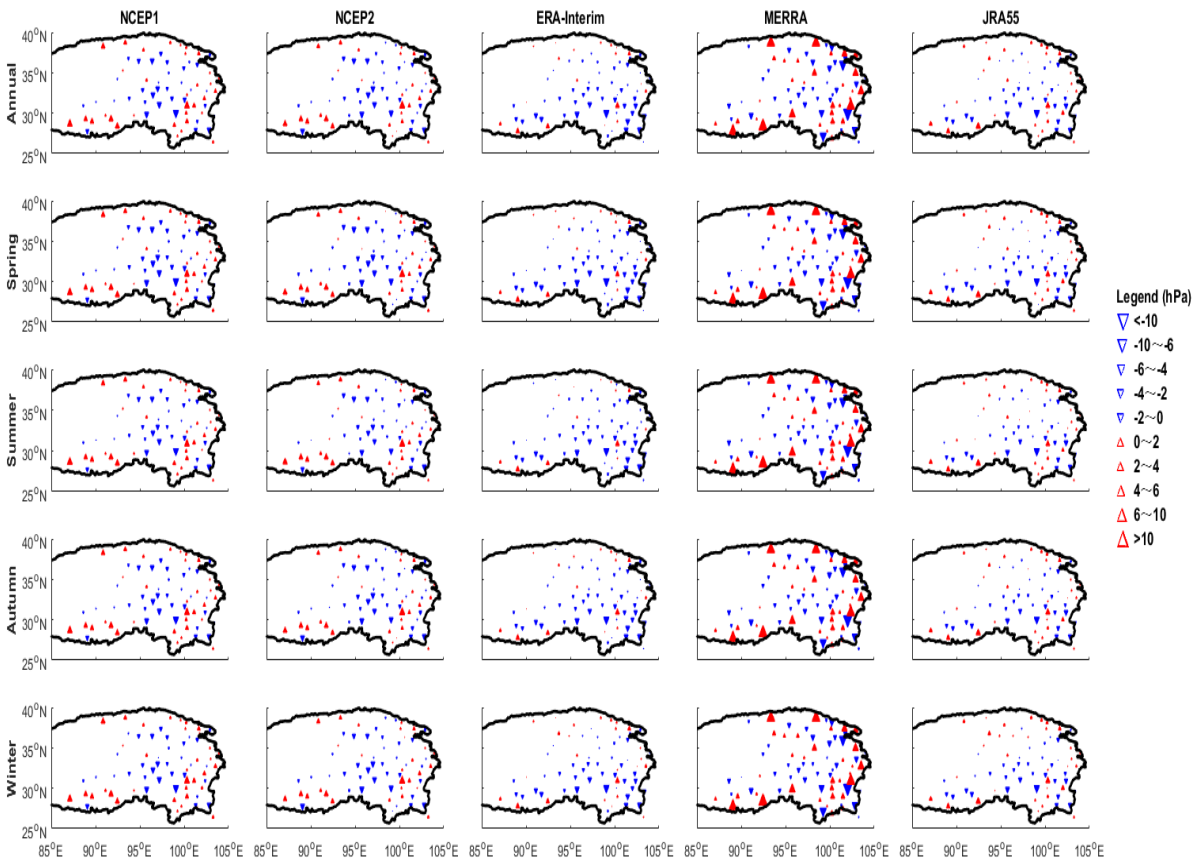

Figure 4. Spatial distribution of mean absolute biases (corrected reanalysis minus observation) of surface pressure over the Tibetan Plateau on an annual (top row) and seasonal basis (other rows). The unit is hPa.

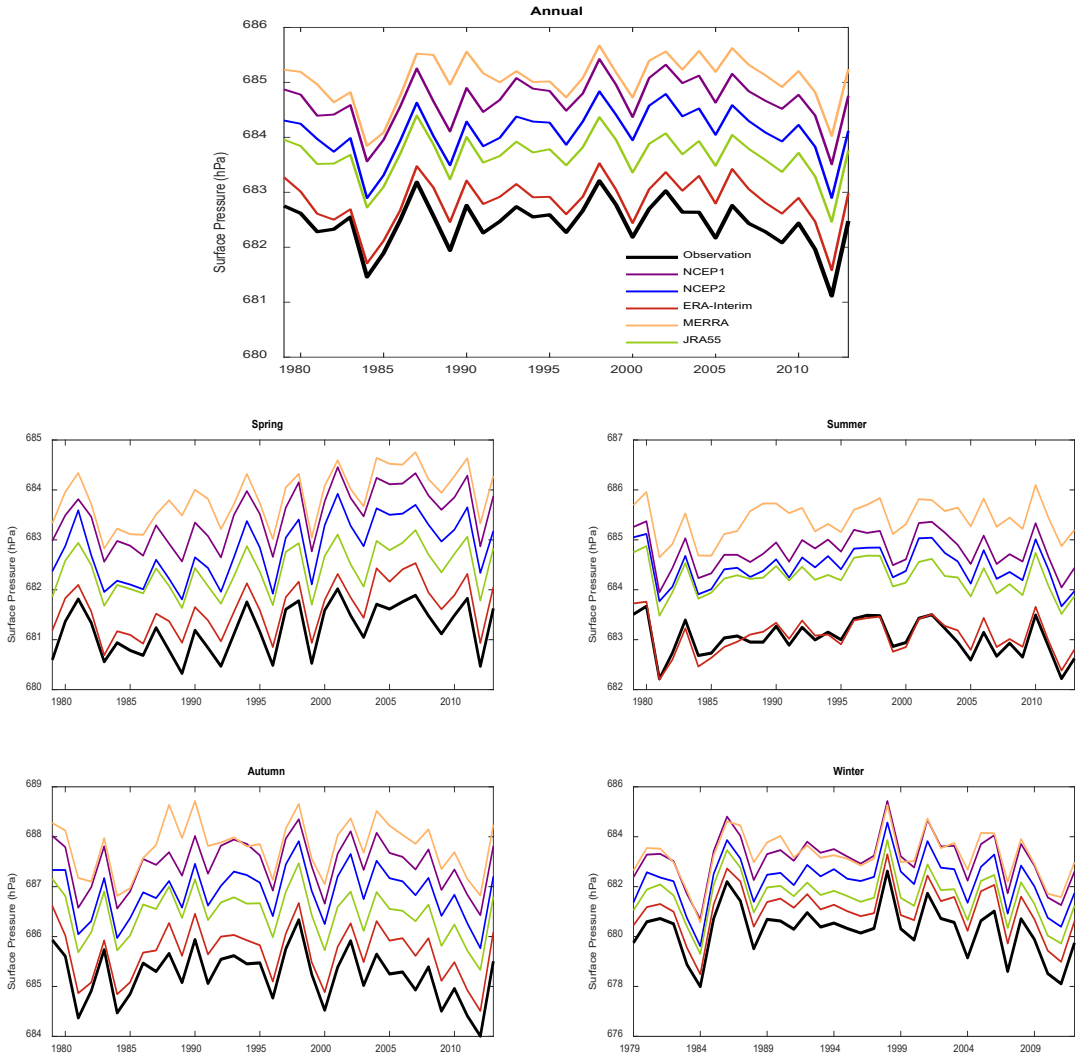

788

789 **Figure 5**. Regional anomaly of surface pressure from observations and each reanalysis

790 (NCEP1, NCEP2, ERA-Interim, MERRA and JRA55) after horizontal bilinear

791 interpolation and corrected by altitude bias over the Tibetan Plateau during 1979–2013

792 on an annual (top panel) and seasonal basis (other four panels).

793

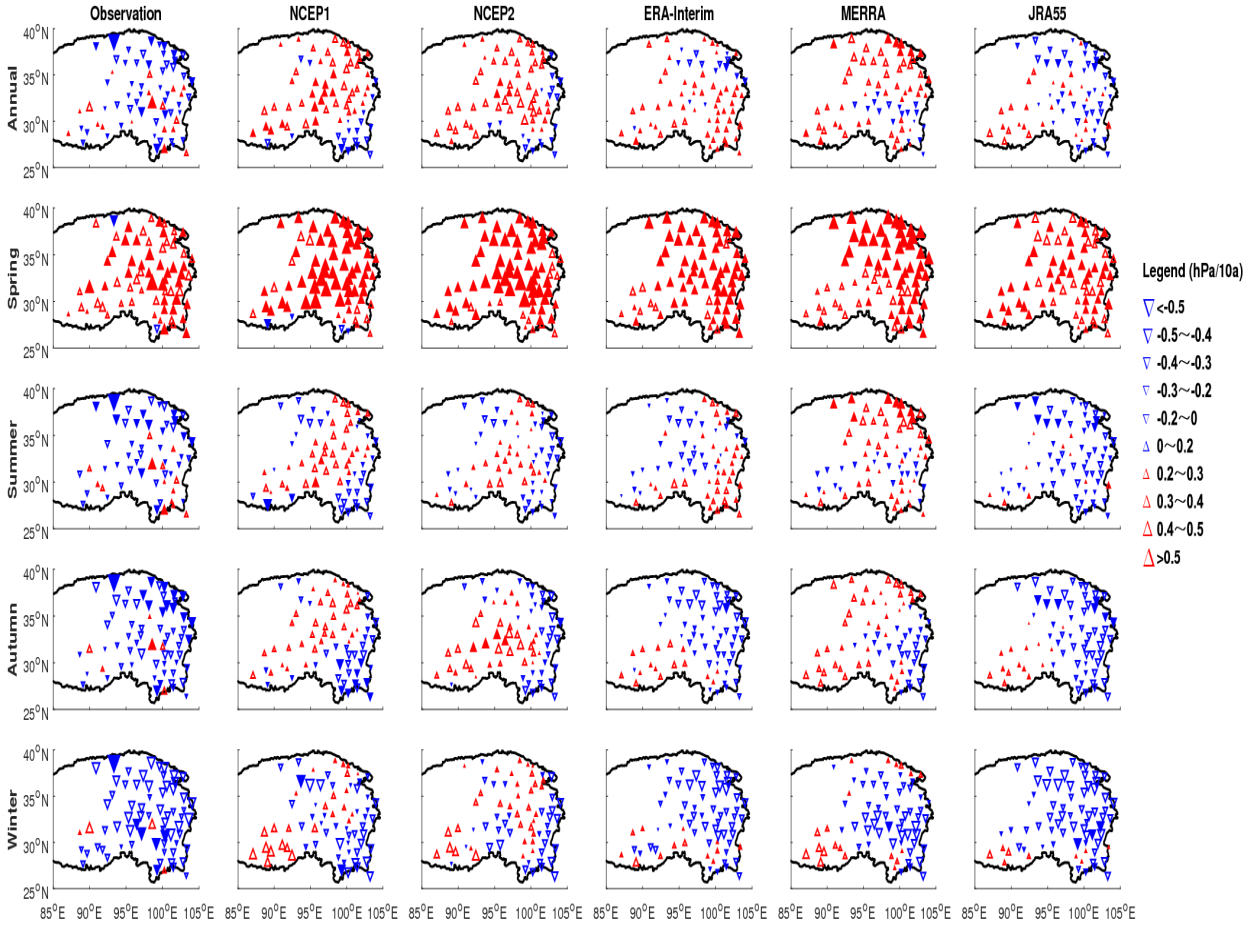

794

795 **Figure 6**. Spatial trends of surface pressure from observations (top left) and the five

796 reanalyses (NCEP1, NCEP2, ERA-Interim, MERRA and JRA55) after correction

797 considering the elevation difference over the Tibetan Plateau during 1979–2013 on an

798 annual and seasonal basis. The unit is hPa/decade. The solid/hollow triangles are the

799 stations with trend passed/failed the significant test.

800

801

802

803

804

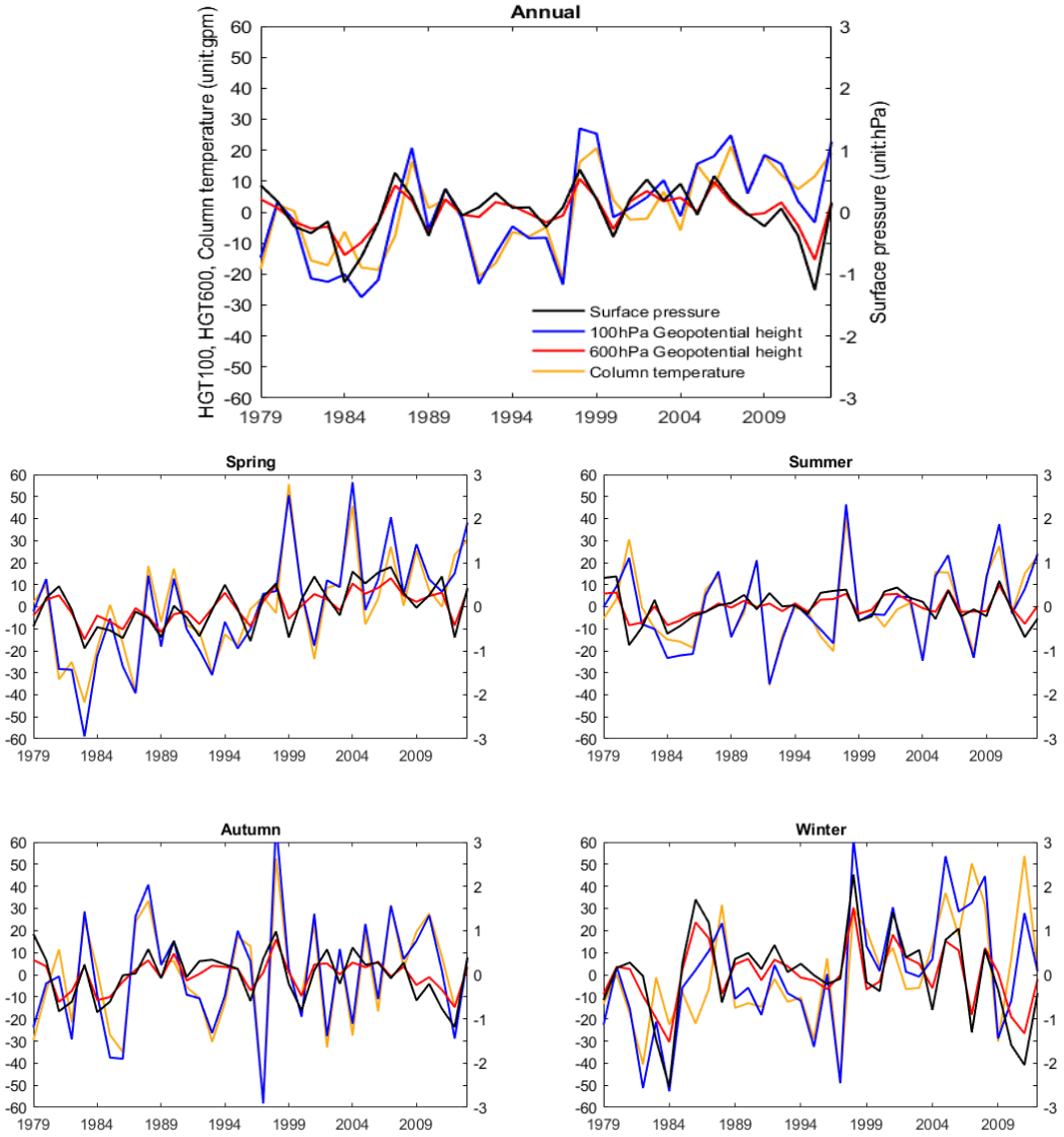

805

806 **Figure 7.** Time series of surface pressure anomalies (black line, hPa), 100 hPa

807 geopotential height (blue line, gpm), 600 hPa geopotential height (red line, gpm), and

808 column temperature (yellow line, °C) over the Tibetan Plateau during 1979–2013 on an

809 annual and seasonal basis based on ERA-Interim dataset.

810

811

812

813

814

815

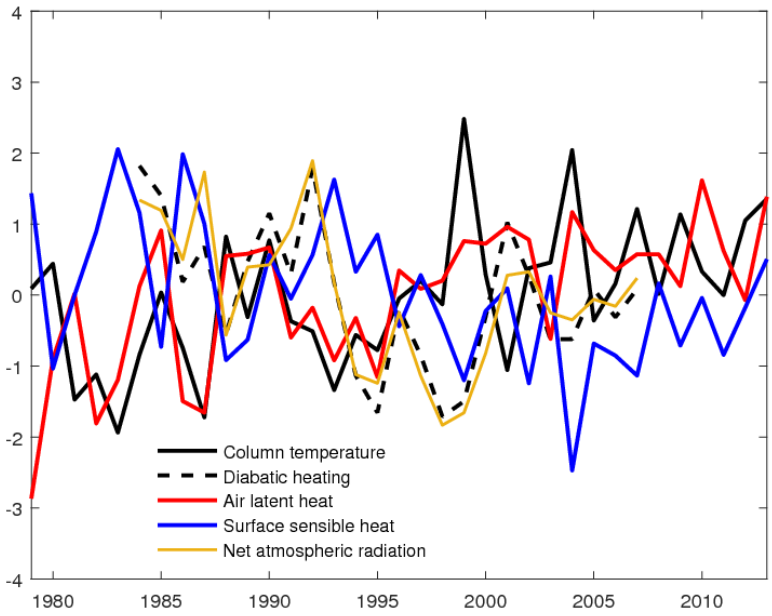

816

817 **Figure 8.** Time series of standardized column air temperature (black solid line), diabatic
818 heating (black dashed line), air latent heat (red solid line), surface sensible heat (blue
819 solid line), and net atmospheric radiation (yellow line) over the Tibetan Plateau during
820 1979–2013 on an annual and seasonal basis based on ERA-Interim dataset. Both net
821 atmospheric radiation and diabatic heating contain the period of 1983-2007, which were
822 obtained from the NASA Langley Research Center Atmospheric Sciences Data Center
823 NASA/GEWEX SRB Project (https://gewex-srb.larc.nasa.gov/).

824

825

826

827

828

829

830

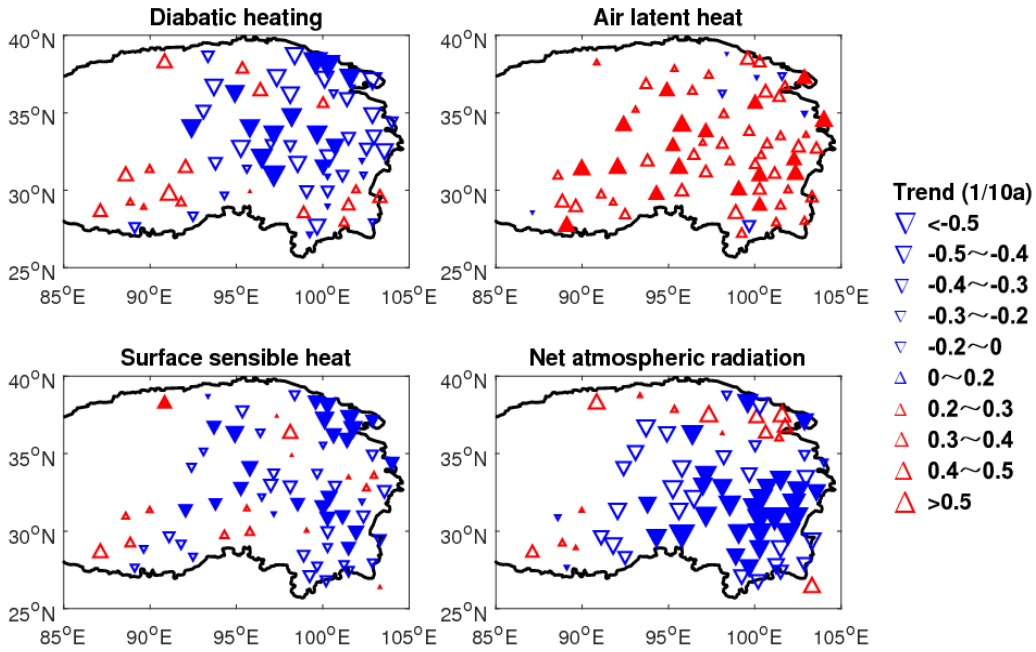

Figure 9. Spatial trends of diabatic heating, air latent heat, surface sensible heat and net atmospheric radiation over the Tibetan Plateau in spring. The solid/hollow triangles are the stations with trend passed/failed the significance test.

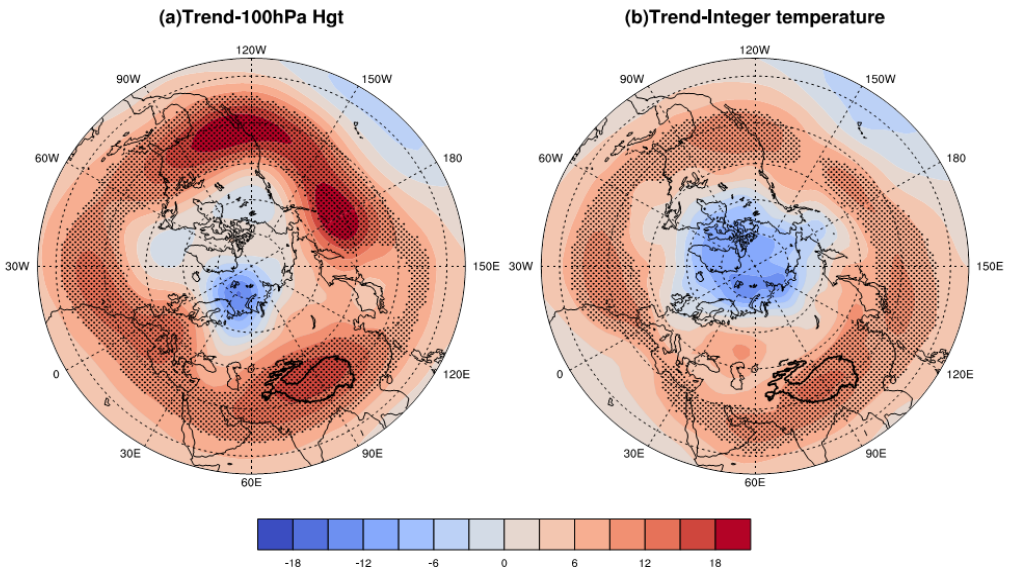

846

847 **Figure 10**. Spatial trends of (a) 100 hPa geopotential height (gpm/decade) and (b)

848 column temperature (°C/decade). The shaded area represents where the trend passed

849 the significant test.

850

851

852

853

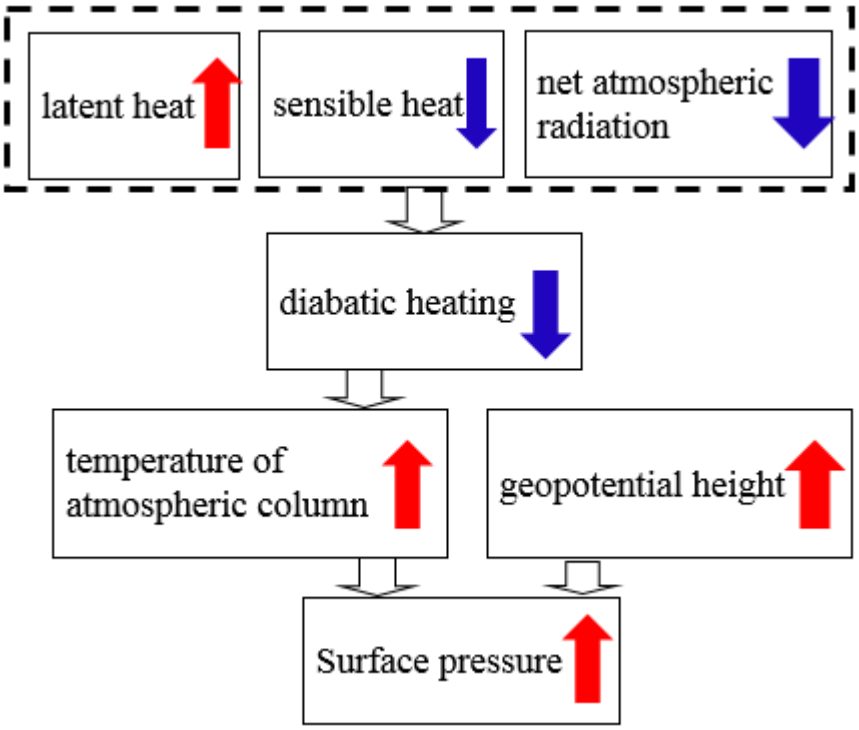

854

855 **Figure 11**. Possible mechanism influencing surface pressure over the Tibetan Plateau

856 in spring. The upward/downward arrows indicate the positive/negative trends, and the

857 size of arrow is proportional to the magnitude of the trends.